nature geoscience

Article

https://doi.org/10.1038/s41561-023-01131-4

Widespread seasonal speed-up of west Antarctic Peninsula glaciers from 2014 to 2021

Received: 15 March 2022

Accepted: 24 January 2023

Published online: 27 February 2023

Check for updates

Benjamin J. Wallis [1] ✉, Anna E. Hogg [1], J. Melchior van Wessem [2], Benjamin J. Davison [1] & Michiel R. van den Broeke [2]

Mass loss from the Antarctic Ice Sheet is dominated by ice dynamics, where ocean-driven melt leads to un-buttressing and ice flow acceleration. Long-term ice speed change has been measured in Antarctica over the past four decades; however, there are limited observations of short-term seasonal speed variability on the grounded ice sheet. Here we assess seasonal variations in ice flow speed on 105 glaciers on the west Antarctic Peninsula using Sentinel-1 satellite observations spanning 2014 to 2021. We find an average summer speed-up of 12.4 ± 4.2%, with maximum speed change of up to 22.3 ± 3.2% on glaciers with the most pronounced seasonality. Our results show that over the six-year study period, glaciers on the west Antarctic Peninsula respond to seasonal forcing in the ice–ocean–atmosphere system, indicating sensitivity to changes in terminus position, surface melt plus rainwater flux, and ocean temperature. Seasonal speed variations must be accounted for when measuring the mass balance and sea level contribution of the Antarctic Peninsula, and studies must establish the future evolution of this previously undocumented signal under climate warming scenarios.

Over the past 25 years the Antarctic Ice Sheet contributed 7.6 ± 3.9 (s.d.) mm to global sea level rise (SLR), with a four-fold increase in the rate of mass loss observed since 1992 (ref. [1]). In Antarctica, mass loss is dominated by ice dynamic processes[2], where acceleration of marine-terminating ice streams is driven by a reduction in resistive force due to ocean-driven ice shelf thinning[3–7], ice shelf disintegration[8], terminus retreat[9,10] and increasing ice damage[11]. Ice speed measurements are a critical dataset for (1) mass balance calculations using the input–output method[12–14]; (2) calibration of models used for projections of future ice sheet evolution[15–17]; and (3) studies to improve our understanding of the physical processes driving ice dynamics and ice–ocean–atmosphere interactions[18,19]. Therefore, generating accurate, high spatial and temporal resolution measurements of this important parameter is essential.

Satellite measurements have documented long-term, multi-year change in ice speed across Antarctica, with the largest accelerations observed in the Amundsen Sea sector[10,14], the Getz basin[20] and on the Antarctic Peninsula (AP)[9,21–23]. However, ice speed can also vary on intra-annual timescales. In Greenland, seasonal ice velocity variations are widespread, caused by basal lubrication from the routing of surface meltwater, and at marine-terminating outlet glaciers in response to change in submarine melt rates and terminus position[24–28]. However, on the Antarctic Ice Sheet there are few observations of widespread seasonal changes in grounded ice speed. Reports of seasonality have been so far limited to two floating ice tongues in East Antarctica[29,30] and glaciers feeding the George VI Ice Shelf[31].

Over the past three decades, the AP has experienced major change. Floating ice shelves have collapsed and retreated[32–34], and the loss of ice shelf buttressing strength has led to an acceleration in ice speed and surface lowering on the grounded ice, increasing ice discharge into the ocean[9,13,35]. Analysis of sediment cores shows that this change

[1]School of Earth and Environment, University of Leeds, Leeds, UK. [2]Institute for Marine and Atmospheric research Utrecht, Utrecht University, Utrecht, Netherlands. ✉e-mail: eebjwa@leeds.ac.uk

https://doi.org/10.1038/s41561-023-01131-4

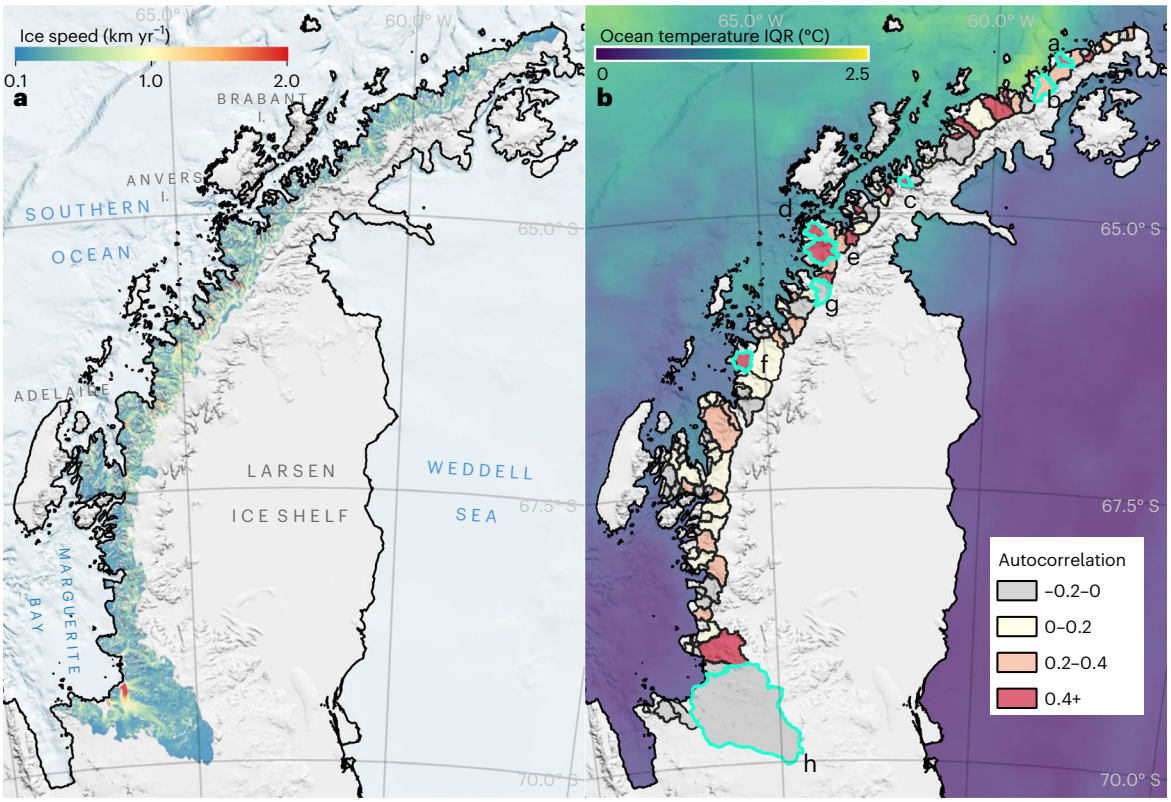

Fig. 1 | West AP ice speed map and ice speed autocorrelation. a, Mean ice speed (km yr^{-1}) on the west AP (December 2014–May 2021). **b**, Glacier drainage basins[70] shaded by the autocorrelation statistic (December 2014–May 2021), which indicates high (red) and low (light grey) annual periodicity in ice speed. Interannual upper-ocean temperature variation is also shown, measured as the annual IQR range of the depth-averaged temperature anomaly from the top 110 m of the water column (2015–2020)[56]. The Reference Elevation Model of Antarctica (REMA) 200 m digital elevation model (DEM) hill-shade[71], coastline (black line) and hill-shade bathymetry from IBSCO v1 (ref. [72]) are shown on both maps for illustrative purposes. Time series are shown in Fig. 2a–h for glaciers highlighted a–h.

is important on the geological timescale, with events of this magnitude not recorded on the AP since the mid-Holocene, or in the case of Larsen B, pre-Holocene[36–38]. Overall, AP glaciers north of 70° S have the potential to increase global mean sea level by 69 ± 5 mm[39], with 7.8% (17,900 km^2) of the AP glaciers thought to be in a state of dynamic imbalance in 2017 (ref. [40]).

The mechanisms driving long-term change on the AP have been attributed to both atmospheric and ocean forcing, with different processes having greater relative importance in different regions. Increased near-surface air temperatures were recorded on the AP in the second half of the twentieth century and linked to ice shelf retreat[41]; however, extending the temperature record into the twenty-first century shows that the warming trend was replaced by a statistically significant period of atmospheric cooling from 1999 to 2014[42]. Despite this long-term cooling trend, air temperatures exceed 0 °C in the summer months, causing widespread surface melt and rain[43–45]. Warm deep ocean water has been linked to terminus retreat on the western AP[46], ice speed increase on the English coast[47], and grounding line retreat on Fleming Glacier[21]. Attribution of causal processes is complex as different forcing mechanisms can dominate at different time periods. On the AP, the role of surface-melt-driven velocity fluctuations has been debated[31,48,49]. Three instances of short-lived (<6 days) speed change were observed simultaneously on four east and one west AP glaciers between October 2016 and April 2018[48]. This was attributed separately to both the lubrication of ice flow following surface meltwater drainage[48], and a surface-melt-induced velocity processing artefact and ocean dynamic forcing[49]. Consequently, further studies are required to improve our understanding of the ice flow response to changing environmental conditions in this region. Here, we use satellite observations to produce a six-year-long record of ice speed measurements on 105 glaciers on the west AP coast, north of the George VI Ice Shelf (Fig. 1a).

Seasonal change in ice speed

Our observations show the spatial distribution of ice velocity across the west AP at 100 m posting (Fig. 1a). We extracted time series of ice speed on 105 glaciers at a location 1 km upstream of the terminus position, which shows an average ice speed of 998 m yr^{-1} and 26 glaciers flowing at speeds of over 1.5 km yr^{-1}. Fast ice flow above 1 km yr^{-1} extends up to 18 km inland on major outlets such as Fleming and Cayley Glaciers, and ice flow is well resolved across the full width of smaller ~1-km-wide flow units with small-scale velocity features such as tributaries also resolved. The ice speed autocorrelation metric, a measure of annual periodicity, shows high values across the west AP, with the largest density of summer speed-up found on glaciers at northern latitudes (Fig. 1b). The ice speed interquartile range (IQR) indicates the amplitude of the change (Extended Data Fig. 2b). This shows that the highest-amplitude seasonal variability is observed on glaciers on the Davis Coast, located to the north of Brabant Island, and near Anvers Island, with different amplitudes of variability observed on neighbouring glaciers. Heterogeneity in the timing and magnitude of speed change between neighbouring glaciers is expected, and has been observed extensively in Greenland and Antarctica[25,28,50,51].

Our velocity time series reveals that seasonal variability in ice speed is widespread across the west AP coast, with a mean summer speed-up of over 10% measured on 76 of the 105 glaciers in the study region (Fig. 2 and Extended Data Fig. 2). Excluding the 27 glaciers that flow at speeds less than 500 m yr^{-1} to avoid undue influence from

https://doi.org/10.1038/s41561-023-01131-4

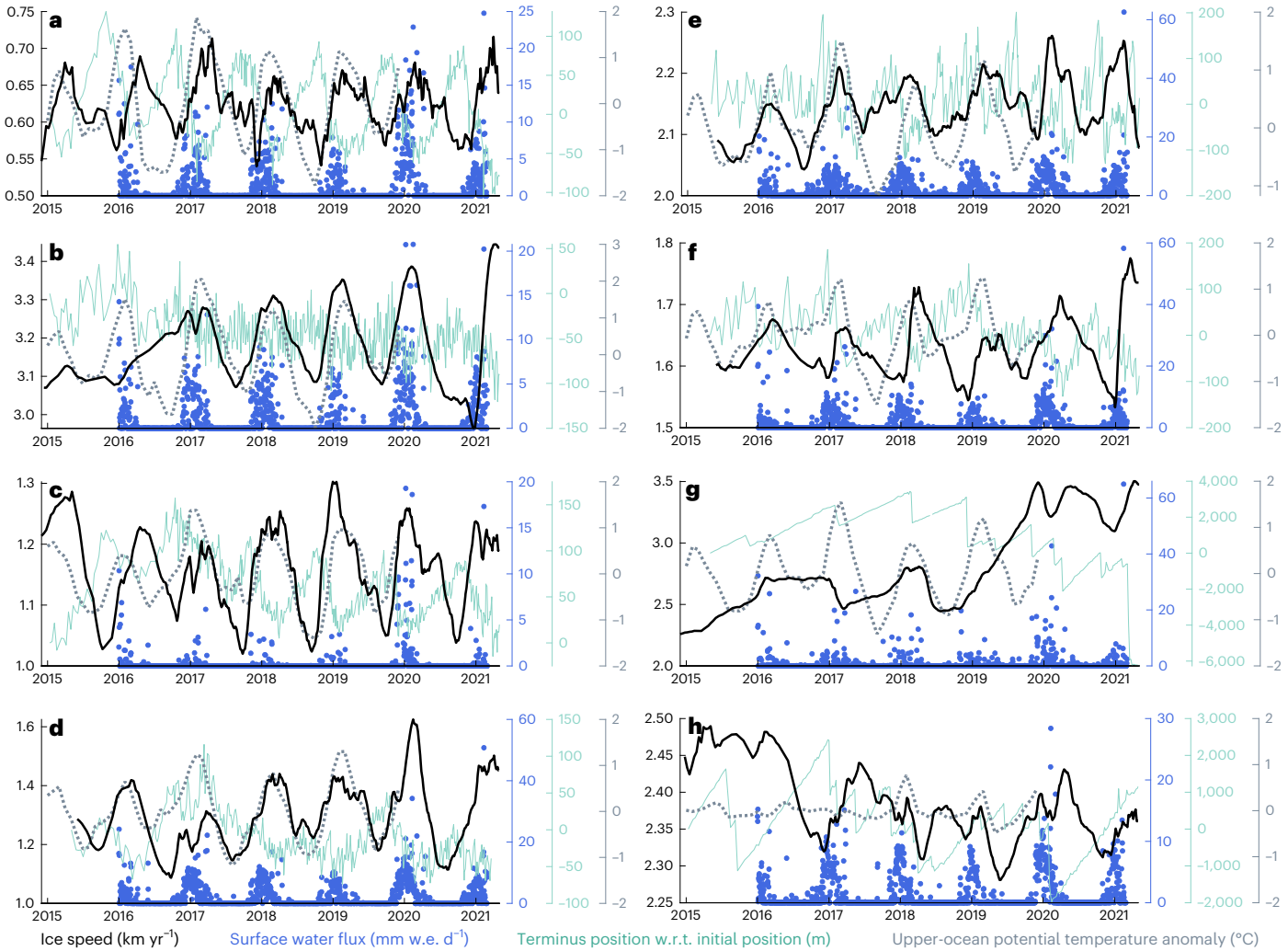

Fig. 2 | Highlight glaciers' time series of ice speed, surface water flux, terminus position and ocean temperature anomaly. a–h, Time series of Kalman-smoothed ice speed (black solid line), RACMO2.3p2 surface water flux (snowmelt plus rain; blue dots)[43,52], terminus position with respect to the final position (green solid line) and upper-ocean (110 m) potential temperature anomaly (grey dashed line)[56]. Time series are shown for unnamed north Bone Bay (**a**), Gavin Ice Piedmont (**b**), Leonardo (**c**), Hotine (**d**), Trooz (**e**), Keith (**f**), Cadman (**g**) and Fleming (**h**) Glaciers. Highlight glaciers in **a**–**f** were selected based on their large seasonal ice speed variability (autocorrelation values of 0.648, 0.314, 0.586, 0.703, 0.575 and 0.575, respectively), to give a spread of locations along the west AP, and to show a range of faster and slower mean ice speeds. w.r.t., with respect to; w.e., water equivalent.

other sources of small-scale variability, such as measurement noise, we observe a mean intra-annual speed variability of 124.2 ± 42.2 m yr^{-1} on the west AP, equivalent to a 12.4 ± 4.2% speed-up during the austral summer. The strongest seasonal cycle is observed on Hotine Glacier (Fig. 2d), located on the Kyiv Peninsula, which speeds up on average by 22.3 ± 3.2% (288.3 ± 41.3 m yr^{-1}) in the summer months compared with its winter minimum. Other glaciers observed to have an extremely pronounced seasonal velocity cycle include the unnamed north Bone Bay glacier, which experienced a mean summer speed-up of 20.2 ± 3.4% (125.6 ± 21.2 m yr^{-1}; Fig. 2a), Gavin Ice Piedmont 6.6 ± 3.1% (211.2 ± 98.7 m yr^{-1}; Fig. 2b), Leonardo Glacier 18.3 ± 2.7% (212.7 ± 31.5 m yr^{-1}; Fig. 2c), Trooz Glacier 5.8 ± 2.4% (123.6 ± 50.5 m yr^{-1}; Fig. 2e) and Keith Glacier 6.6 ± 3.3% (107.8 ± 54.2 m yr^{-1}; Fig. 2f). On the glaciers shown in Fig. 2a–f, seasonal ice speed variability is observed between 2 and 5 km inland of the terminus (Extended Data Fig. 4).

Long-term ice dynamic response

In addition to widespread short-term seasonal ice speed variability, our results also show newly observed longer-term, multi-annual ice dynamic signals on west AP glaciers. Most notably, Cadman Glacier (Fig. 2g) located in Beascochea Bay accelerated by 1.05 ± 0.07 km yr^{-1} (42.9 ± 2.7%) in 2019. Splettstoesser Glacier located on the Stresher Peninsula exhibited a multi-year slowdown of 315 ± 20 m yr^{-1} (35.9 ± 2.3%) over the full six-year study period; and Otlet Glacier, which flows into the Grandidier Channel, experienced a multi-year acceleration of 278 ± 26 m yr^{-1} (38.4 ± 3.6%) between 2014 and 2021. While Fleming Glacier exhibits a clear seasonal ice speed signal, our velocity time series shows that this is imposed on top of the longer-term ice dynamic trend (Fig. 2h), which reached its peak speed of 2.9 km yr^{-1} in 2012 (ref. [21]).

Influence of external forcing mechanisms

We investigated the influence of external forcing mechanisms and change in calving front location on eight highlight glaciers, which are spatially distributed across the study area (Figs. 1b and 2a–h). Glaciers with pronounced seasonal ice speed variability during the study period were selected (Fig. 2a–f), along with regions where a longer-term ice dynamic response was observed, as seen on Cadman (Fig. 2g) and Fleming Glaciers (Fig. 2h).

We assessed the availability of surface water on the west AP by extracting daily estimates of snowmelt and rainfall from a regional

https://doi.org/10.1038/s41561-023-01131-4

climate model (RACMO2.3p2 (refs. [43,45,52]); Fig. 2a–h). The results show that on the AP the summer melt season lasts four to five months, with snowmelt starting in October and peaking in December and January. Substantial late-season surface melt days occur throughout February and, in some areas, into March. This is consistent with microwave scatterometer and modelling studies showing persistent melt durations in excess of 100 days on the AP[44]. Larger volumes of surface melt and precipitation are found at the northern tip of the AP[43], where seasonal speed variations were strongest (Fig. 1b and Extended Data Fig. 2b). Rainfall in the late austral summer (January to April) extends the period where liquid water is available at a time when other sources of surface-derived meltwater are decreasing. Our results show that on the six highlight glaciers with pronounced seasonal ice speed variability, the seasonal speed-up roughly coincided with the onset of surface melting each year; however, the highest ice speeds generally occur several weeks after the peak in surface water supply (Figs. 2a–f and 3). Further analysis of modelled runoff at the basin scale shows that on the west AP, runoff lags surface meltwater and rain flux by several weeks (Extended Data Fig. 5) and peaks in February for the period July 2016–July 2021, coinciding directly with the peak in ice speed (Fig. 3). We therefore attribute this lag to the time taken for the water to percolate through the firn layer of the west AP, which can be up to 100 m thick[53]. Modelling predicts the presence of perennial firn aquifers on the west AP[54], which may provide a mechanism for modulating the supply of meltwater to the bed throughout the year. On the 20 glaciers with the strongest annual ice speed periodicity (highest autocorrelation values), we recorded the largest average seasonal speed variability (167.4 ± 40.0 m yr^{-1}) during our study period in the 2019/2020 austral summer, when record high surface melt was observed on the AP[55]. This indicates that the largest seasonal speed-up occurs in years with most surface melt. The spatial distribution of strong surface melt and the temporally coincident peak in runoff with the highest annual summer speeds indicates a link with hydrologically driven basal lubrication on west AP glaciers.

Ocean temperature data from a reanalysis model[56] were used to assess the spatially variable pattern of integrated ocean heat variability in the top 110 m of the water column in the Bellingshausen Sea, between 2015 and 2020 (Fig. 1b). Our results show that there is a strong seasonal signal in the temperature anomaly, with mean seasonal variability of 1.9 °C recorded in the Bellingshausen Sea north of Adelaide Island, and maximum local change of up to 3.1 °C found at the tip of the AP north of the Davis Coast (Fig. 1b). Our ice speed time series show that on seven of the eight highlight glaciers there is a strong correspondence between the timing of the seasonal ice speed-up and ocean temperature increase (Fig. 2a–g). The exception to this is in Marguerite Bay next to Fleming Glacier, where there is no strong seasonality in the ocean temperature anomaly (Fig. 2h). Previous studies have shown that persistent sea-ice cover in this area[57] acts as a thermal barrier, preventing warming of surface waters in the summer and heat loss to the atmosphere in the winter, as observed previously in Ryder Bay[58].

Change in calving front location

We exploited the full Sentinel-1 archive to measure change in terminus position on all eight highlight glaciers throughout the six-year study period (Fig. 2a–h)[59]. In all cases, we observe seasonal variability in the terminus position with maximum advance in winter or early spring and retreat during the summer, with the most pronounced change in terminus position observed on slower-flowing glaciers (Fig. 2a,c). On the six glaciers with strong seasonal ice speed periodicity (Fig. 2a–f), the terminus position retreated inland during the summer months by 117 m on average, with a minimum and maximum summer retreat of 35 m and 254 m measured on Gavin Ice Piedmont and Trooz Glacier, respectively.

We observed a multi-annual change in terminus position on Cadman Glacier, where the terminus retreated by 10 km over a two-year period, between its most advanced position in February 2019 and the final measured position in May 2021 (Fig. 2e). This change corresponded with a major and sustained 1.04 km yr^{-1} (42.0%) increase in ice speed that started in October 2018. The observed speed-up started two months prior to the onset of sustained terminus retreat, suggesting that an un-buttressing occurred first, followed by the resulting acceleration and terminus retreat. Our results show that Fleming Glacier experienced a pattern of winter terminus advance and summer retreat caused by large calving events over the six-year study period. In 2020, the peak summer speed of 2.43 km yr^{-1} was recorded in April following a 2.16 km calving front retreat event in February 2020 (Fig. 2h). This suggests that the speed of Fleming Glacier is strongly dependant on the terminus position, on intra-annual timescales, with sensitivity to change enhanced by its retrograde bed slope geometry[21,60].

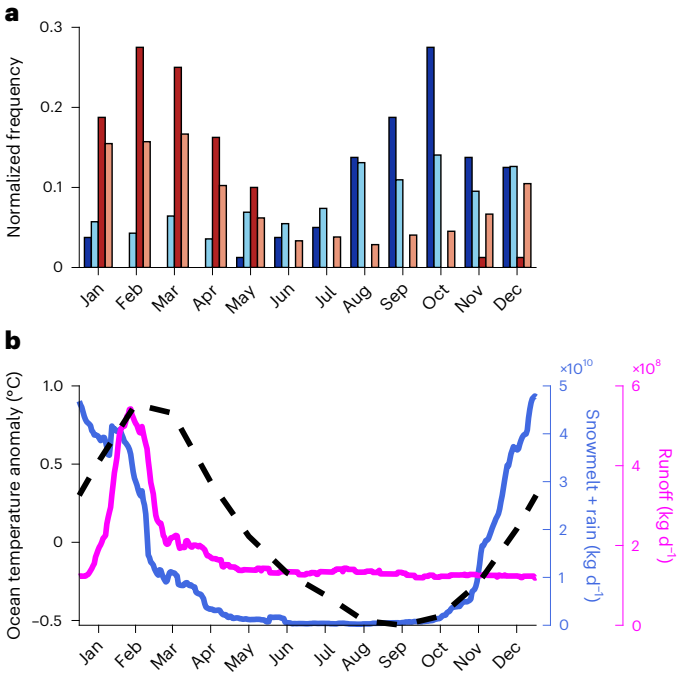

Fig. 3 | Annual distribution of speed maximums and environmental forcings. **a**, Histogram of the month of velocity maximum (reds) and velocity minimum (blues) on all glaciers (light shading) and top 20 glaciers by autocorrelation (dark shading). **b**, West AP basin total modelled snowmelt plus rain (blue) and runoff (mauve) from RACMO2.3p2 (refs. [43,52]), and monthly mean ocean temperature anomaly (°C) for all sample points (black dashed line)[56]. Both plots cover the period of full availability for all datasets: July 2016 to July 2020.

Discussion

We further assessed the role of external forcing mechanisms as a driver of seasonal change by comparing the monthly distribution of annual maximum and minimum ice speeds on all 105 glaciers, with the monthly distribution of mean surface water flux and ocean temperature anomaly averaged across the full period of data availability (Fig. 3). The results show a clear seasonal distribution of both ice speed and external forcing over the whole west AP study region, with speed minimums recorded between September and October each year before the summer season starts, and maximum speeds occurring from February to April each year when surface water supply and ocean temperature are higher. This shows that either individually or in combination, meltwater-induced changes in basal effective pressure and ocean-temperature-induced changes in terminus ablation rates are at least partially responsible for the observed changes in ice speed. At seven of the eight highlight glaciers, we also find a clear correspondence between seasonal terminus position change, potentially driven by ocean temperature changes,

and ice speed (Fig. 2a–g). This monthly distribution is even more pronounced if only the 20 glaciers with the strongest annual periodicity in ice speed are assessed (Fig. 3).

While the size of a glacier's ice dynamic response will be in part controlled by the strength of the environmental forcing, the sensitivity of an individual glacier to respond is controlled by glacier geometry[61] and subglacial conditions[50]. Mechanistically, the observed seasonal speed fluctuations must be driven by changes in buttressing force and/or basal sliding. On seasonal timescales, the buttressing force can be reduced by terminus retreat during the summer; however, this must itself be driven by an increase in ice front ablation caused by environmental factors. In Svalbard and the AP, upper-ocean temperature is strongly linked to high rates of ablation at the terminus of tidewater glaciers[62,63]. Our results show that glaciers with the largest seasonal speed variability undergo substantial terminus position change and are adjacent to ocean water with the greatest seasonal ocean temperature variability, which is strongest at the northern tip of the west AP (Figs. 1b and 2a–f). This provides a mechanism for seasonal ice speed fluctuations on the west AP to be forced by ocean-temperature-induced frontal retreat.

Meltwater penetration to the glacier bed can reduce basal traction and cause hydraulic jacking, both of which induce ice speed-up. Our regional climate model results show high summertime water flux at the surface corresponding to observations of summertime ice speed-up, and that a lag between the peak surface melt and peak summer ice speed-up can be explained by the time required for surface water to percolate through the snowpack as runoff (Fig. 3). Interannual variability in the magnitude of seasonal speed-up may also be explained by surface water availability, as the year with the most surface melt (2019/20) coincided with the year with the largest seasonal speed-up on many glaciers in the study area. Sparse field studies have observed glacial sediment plumes on the west AP coast, providing further evidence that meltwater reaches the subglacial drainage system in this region[64,65]. While future studies must seek to partition the relative importance of different forcing mechanisms on individual glaciers, we can conclude that the seasonal ice speed changes we observe on the west AP are due to increased heat in the ice–atmosphere–ocean system forcing glacier dynamics.

Our results are important for mass balance studies where the input–output method is used[1,13], because seasonal change in ice speed causes a seasonal variation in ice discharge. If summer ice speed is assumed to be representative of the annual mean, this leads to an overestimation of the ice discharge and consequently a negative bias in the mass balance assessments. We quantify the impact of this bias on mass balance by calculating ice discharge for the six highlight glaciers (Fig. 2a–f), using the full time series of seasonally variable ice speed, and with a linear interpolation between summer maximum speeds. Our results show that for these glaciers, when summer speeds alone are used, the ice discharge is overestimated by 7.2% on average, with the mass balance 30.2% more negative than it would be if seasonal speed variability is accounted for (Extended Data Table 1).

We observe strong seasonal flow variability during our six-year study period, but our results do not show the timing of its onset. The AP experienced the greatest warming of any Southern Hemisphere terrestrial region in the later twentieth century[66,67]; however, air temperatures decreased from the late 1990s to 2014 (ref. [42]). Surface water flux data from RACMO shows that between 1979 and 2019, meltwater forcing has been at current or higher levels throughout the 40-year period, suggesting seasonal ice speed changes on the west AP could have been present in previous decades. In the future, atmospheric temperatures on the AP are projected to rise under a 1.5 °C warming scenario[67], the availability of surface meltwater is projected to double by 2050 independent of the climate scenario[68] and precipitation is projected to increase[69], all affecting the seasonal forcing applied to glaciers in the region and their mass balance. Future studies should combine in-situ measurements with satellite observations to further investigate the complex link between ice speed, surface melt and ocean temperature variability across the west AP, and to assess their relative importance at the glacier basin scale. Long- and short-term ice dynamic trends must be monitored and understood, with the large number of AP glaciers and the variety of responses providing a natural laboratory that can be used to improve our understanding of the processes driving present-day ice loss in Antarctica. Substantial differences remain between estimates of the sea level contribution from the AP made using independent techniques[1], and our results show that accounting for seasonal speed variations may enable a proportion of that difference to be reconciled.

Online content

Any methods, additional references, Nature Portfolio reporting summaries, source data, extended data, supplementary information, acknowledgements, peer review information; details of author contributions and competing interests; and statements of data and code availability are available at https://doi.org/10.1038/s41561-023-01131-4.

References

1. Shepherd, A. et al. Mass balance of the Antarctic Ice Sheet from 1992 to 2017. *Nature* **558**, 219–222 (2018).
2. Slater, T., Hogg, A. E. & Mottram, R. Ice-sheet losses track high-end sea-level rise projections. *Nat. Clim. Change* **10**, 879–881 (2020).
3. Dutrieux, P. et al. Strong sensitivity of Pine Island Ice-Shelf melting to climatic variability. *Science* **343**, 174–178 (2014).
4. Christianson, K. et al. Sensitivity of Pine Island Glacier to observed ocean forcing. *Geophys. Res. Lett.* **43**, 10817–10825 (2016).
5. Jenkins, A. et al. West Antarctic Ice Sheet retreat in the Amundsen Sea driven by decadal oceanic variability. *Nat. Geosci.* **11**, 733–738 (2018).
6. Reese, R., Albrecht, T., Mengel, M., Asay-Davis, X. & Winkelmann, R. Antarctic sub-shelf melt rates via PICO. *Cryosphere* **12**, 1969–1985 (2018).
7. Gudmundsson, G. H., Paolo, F. S., Adusumilli, S. & Fricker, H. A. Instantaneous Antarctic ice sheet mass loss driven by thinning ice shelves. *Geophys. Res. Lett.* **46**, 13903–13909 (2019).
8. Scambos, T. A., Bohlander, J. A., Shuman, C. A. & Skvarca, P. Glacier acceleration and thinning after ice shelf collapse in the Larsen B embayment, Antarctica. *Geophys. Res. Lett.* **31**, L18402 (2004).
9. Rignot, E. et al. Accelerated ice discharge from the Antarctic Peninsula following the collapse of Larsen B Ice Shelf. *Geophys. Res. Lett.* **31**, L18401 (2004).
10. Joughin, I., Shapero, D., Smith, B., Dutrieux, P. & Barham, M. Ice-shelf retreat drives recent Pine Island Glacier speedup. *Sci. Adv.* **7**, eabg3080 (2021).
11. Lhermitte, S. et al. Damage accelerates ice shelf instability and mass loss in Amundsen Sea Embayment. *Proc. Natl Acad. Sci. USA* **117**, 24735–24741 (2020).
12. Rott, H., Müller, F., Nagler, T. & Floricioiu, D. The imbalance of glaciers after disintegration of Larsen-B Ice Shelf, Antarctic Peninsula. *Cryosphere* **5**, 125–134 (2011).
13. Rott, H. et al. Changing pattern of ice flow and mass balance for glaciers discharging into the Larsen A and B embayments, Antarctic Peninsula, 2011 to 2016. *Cryosphere* **12**, 1273–1291 (2018).
14. Mouginot, J., Rignot, E. & Scheuchl, B. Sustained increase in ice discharge from the Amundsen Sea Embayment, West Antarctica, from 1973 to 2013. *Geophys. Res. Lett.* **41**, 1576–1584 (2014).
15. Alley, R. B., Clark, P. U., Huybrechts, P. & Joughin, I. Ice-sheet and sea-level changes. *Science* **310**, 456–460 (2005).

16. Barrand, N. E. et al. Computing the volume response of the Antarctic Peninsula ice sheet to warming scenarios to 2200. *J. Glaciol.* **59**, 397–409 (2013).
17. Cornford, S. L. et al. Century-scale simulations of the response of the West Antarctic Ice Sheet to a warming climate. *Cryosphere* **9**, 1579–1600 (2015).
18. Rignot, E., Mouginot, J. & Scheuchl, B. Ice flow of the Antarctic Ice Sheet. *Science* **333**, 1427–1430 (2011).
19. Scambos, T. A., Berthier, E. & Shuman, C. A. The triggering of subglacial lake drainage during rapid glacier drawdown: Crane Glacier, Antarctic Peninsula. *Ann. Glaciol.* **52**, 74–82 (2011).
20. Selley, H. L. et al. Widespread increase in dynamic imbalance in the Getz region of Antarctica from 1994 to 2018. *Nat. Commun.* **12**, 1133 (2021).
21. Friedl, P., Seehaus, T. C., Wendt, A., Braun, M. H. & Höppner, K. Recent dynamic changes on Fleming Glacier after the disintegration of Wordie Ice Shelf, Antarctic Peninsula. *Cryosphere* **12**, 1347–1365 (2018).
22. Pritchard, H. D. & Vaughan, D. G. Widespread acceleration of tidewater glaciers on the Antarctic Peninsula. *J. Geophys. Res. Earth Surf.* **112**, F03S29 (2007).
23. Seehaus, T., Cook, A. J., Silva, A. B. & Braun, M. Changes in glacier dynamics in the northern Antarctic Peninsula since 1985. *Cryosphere* **12**, 577–594 (2018).
24. Joughin, I. et al. Seasonal speedup along the western flank of the Greenland Ice Sheet. *Science* **320**, 781–783 (2008).
25. Moon, T. et al. Distinct patterns of seasonal Greenland glacier velocity. *Geophys. Res. Lett.* **41**, 7209–7216 (2014).
26. Moon, T., Joughin, I. & Smith, B. Seasonal to multiyear variability of glacier surface velocity, terminus position, and sea ice/ice mélange in northwest Greenland. *J. Geophys. Res. Earth Surf.* **120**, 818–833 (2015).
27. Sundal, A. V. et al. Melt-induced speed-up of Greenland Ice Sheet offset by efficient subglacial drainage. *Nature* **469**, 521–524 (2011).
28. Vijay, S. et al. Resolving seasonal ice velocity of 45 Greenlandic glaciers with very high temporal details. *Geophys. Res. Lett.* **46**, 1485–1495 (2019).
29. Greene, C. A., Young, D. A., Gwyther, D. E., Galton-Fenzi, B. K. & Blankenship, D. D. Seasonal dynamics of Totten Ice Shelf controlled by sea ice buttressing. *Cryosphere* **12**, 2869–2882 (2018).
30. Liang, Q. et al. Ice flow variations at Polar Record Glacier, East Antarctica. *J. Glaciol.* **65**, 279–287 (2019).
31. Boxall, K., Christie, F. D. W., Willis, I. C., Wuite, J. & Nagler, T. Seasonal land-ice-flow variability in the Antarctic Peninsula. *Cryosphere* **16**, 3907–3932 (2022).
32. Cook, A. J. & Vaughan, D. G. Overview of areal changes of the ice shelves on the Antarctic Peninsula over the past 50 years. *Cryosphere* **4**, 77–98 (2010).
33. Rott, H., Skvarca, P. & Nagler, T. Rapid collapse of northern Larsen Ice Shelf, Antarctica. *Science* **271**, 788–792 (1996).
34. Rack, W. & Rott, H. Pattern of retreat and disintegration of the Larsen B Ice Shelf, Antarctic Peninsula. *Ann. Glaciol.* **39**, 505–510 (2004).
35. Seehaus, T. C. et al. Dynamic response of Sjögren inlet glaciers, Antarctic Peninsula, to ice shelf breakup derived from multi-mission remote sensing time series. *Front. Earth Sci.* **4**, 66 (2016).
36. Brachfeld, S. et al. Holocene history of the Larsen-A Ice Shelf constrained by geomagnetic paleointensity dating. *Geology* **31**, 749–752 (2003).
37. Pudsey, C. J. & Evans, J. First survey of Antarctic sub–ice shelf sediments reveals mid-Holocene ice shelf retreat. *Geology* **29**, 787–790 (2001).
38. Domack, E. et al. Stability of the Larsen B Ice Shelf on the Antarctic Peninsula during the Holocene epoch. *Nature* **436**, 681–685 (2005).
39. Huss, M. & Farinotti, D. A high-resolution bedrock map for the Antarctic Peninsula. *Cryosphere* **8**, 1261–1273 (2014).
40. Shepherd, A. et al. Trends in Antarctic Ice Sheet elevation and mass. *Geophys. Res. Lett.* **46**, 8174–8183 (2019).
41. Vaughan, D. G. & Doake, C. S. M. Recent atmospheric warming and retreat of ice shelves on the Antarctic Peninsula. *Nature* **379**, 328–331 (1996).
42. Turner, J. et al. Absence of 21st century warming on Antarctic Peninsula consistent with natural variability. *Nature* **535**, 411–415 (2016).
43. van Wessem, J. M. et al. The modelled surface mass balance of the Antarctic Peninsula at 5.5 km horizontal resolution. *Cryosphere* **10**, 271–285 (2016).
44. Barrand, N. E. et al. Trends in Antarctic Peninsula surface melting conditions from observations and regional climate modeling. *J. Geophys. Res. Earth Surf.* **118**, 315–330 (2013).
45. van Wessem, J. M., Meredith, M. P., Reijmer, C. H., van den Broeke, M. R. & Cook, A. J. Characteristics of the modelled meteoric freshwater budget of the western Antarctic Peninsula. *Deep Sea Res. II* **139**, 31–39 (2017).
46. Cook, A. J. et al. Ocean forcing of glacier retreat in the western Antarctic Peninsula. *Science* **353**, 283–286 (2016).
47. Hogg, A. E. et al. Increased ice flow in Western Palmer Land linked to ocean melting. *Geophys. Res. Lett.* **44**, 4159–4167 (2017).
48. Tuckett, P. et al. Rapid accelerations of Antarctic Peninsula outlet glaciers driven by surface melt. *Nat. Commun.* **10**, 4311 (2019).
49. Rott, H. et al. Impact of marine processes on flow dynamics of northern Antarctic Peninsula outlet glaciers. *Nat. Commun.* **11**, 2969 (2020).
50. Davison, B. J. et al. Subglacial drainage evolution modulates seasonal ice flow variability of three tidewater glaciers in southwest Greenland. *J. Geophys. Res. Earth Surf.* **125**, e2019JF005492 (2020).
51. Konrad, H. et al. Uneven onset and pace of ice-dynamical imbalance in the Amundsen Sea Embayment, West Antarctica. *Geophys. Res. Lett.* **44**, 910–918 (2017).
52. van Wessem, J. M. et al. Modelling the climate and surface mass balance of polar ice sheets using RACMO2 – Part 2: Antarctica (1979–2016). *Cryosphere* **12**, 1479–1498 (2018).
53. Veldhuijsen, S. B. M., van de Berg, W. J., Brils, M., Kuipers Munneke, P. & van den Broeke, M. R. Characteristics of the contemporary Antarctic firn layer simulated with IMAU-FDM v1.2A (1979–2020). Preprint at *Cryosphere Discuss.* https://doi.org/10.5194/tc-2022-118 (2022).
54. van Wessem, J. M., Steger, C. R., Wever, N. & van den Broeke, M. R. An exploratory modelling study of perennial firn aquifers in the Antarctic Peninsula for the period 1979–2016. *Cryosphere* **15**, 695–714 (2021).
55. Banwell, A. F. et al. The 32-year record-high surface melt in 2019/2020 on the northern George VI Ice Shelf, Antarctic Peninsula. *Cryosphere* **15**, 909–925 (2021).
56. Jean-Michel, L. et al. The Copernicus global 1/12° oceanic and sea ice GLORYS12 reanalysis. *Front. Earth Sci.* **9**, 698876 (2021).
57. Stammerjohn, S. E., Martinson, D. G., Smith, R. C. & Iannuzzi, R. A. Sea ice in the western Antarctic Peninsula region: spatio-temporal variability from ecological and climate change perspectives. *Deep Sea Res. II* **55**, 2041–2058 (2008).
58. Venables, H. J. & Meredith, M. P. Feedbacks between ice cover, ocean stratification, and heat content in Ryder Bay, western Antarctic Peninsula. *J. Geophys. Res. Oceans* **119**, 5323–5336 (2014).

59. Lea, J. M. The Google Earth Engine Digitisation Tool (GEEDiT) and the Margin Change Quantification Tool (MaQiT) – simple tools for the rapid mapping and quantification of changing Earth surface margins. *Earth Surf. Dyn.* **6**, 551–561 (2018).
60. Howat, I. M., Joughin, I., Fahnestock, M., Smith, B. E. & Scambos, T. A. Synchronous retreat and acceleration of southeast Greenland outlet glaciers 2000–06: ice dynamics and coupling to climate. *J. Glaciol.* **54**, 646–660 (2008).
61. Frank, T., Åkesson, H., de Fleurian, B., Morlighem, M. & Nisancioglu, K. H. Geometric controls of tidewater glacier dynamics. *Cryosphere* **16**, 581–601 (2022).
62. Luckman, A. et al. Calving rates at tidewater glaciers vary strongly with ocean temperature. *Nat. Commun.* **6**, 8566 (2015).
63. Dryak, M. C. & Enderlin, E. M. Analysis of Antarctic Peninsula glacier frontal ablation rates with respect to iceberg melt-inferred variability in ocean conditions. *J. Glaciol.* **66**, 457–470 (2020).
64. Rodrigo, C., Giglio, S. & Varas, A. Glacier sediment plumes in small bays on the Danco Coast, Antarctic Peninsula. *Antarct. Sci.* **28**, 395–404 (2016).
65. Rodrigo, C., Varas-Gómez, A., Bustamante-Maino, A. & Mena-Hodges, E. High-concentration sediment plumes, Horseshoe Island, western Antarctic Peninsula. *Antarct. Sci.* **33**, 213–216 (2021).
66. Turner, J. et al. Antarctic climate change during the last 50 years. *Int. J. Climatol.* **25**, 279–294 (2005).
67. Siegert, M. et al. The Antarctic Peninsula under a 1.5 °C global warming scenario. *Front. Environ. Sci.* **7**, 102 (2019).
68. Trusel, L. D. et al. Divergent trajectories of Antarctic surface melt under two twenty-first-century climate scenarios. *Nat. Geosci.* **8**, 927–932 (2015).
69. Krinner, G., Magand, O., Simmonds, I., Genthon, C. & Dufresne, J.-L. Simulated Antarctic precipitation and surface mass balance at the end of the twentieth and twenty-first centuries. *Clim. Dyn.* **28**, 215–230 (2007).
70. Cook, A. J., Vaughan, D. G., Luckman, A. J. & Murray, T. A new Antarctic Peninsula glacier basin inventory and observed area changes since the 1940s. *Antarct. Sci.* **26**, 614–624 (2014).
71. Howat, I. M., Porter, C., Smith, B. E., Noh, M.-J. & Morin, P. The reference elevation model of Antarctica. *Cryosphere* **13**, 665–674 (2019).
72. Arndt, J. E. et al. The International Bathymetric Chart of the Southern Ocean (IBCSO) Version 1.0—a new bathymetric compilation covering circum-Antarctic waters. *Geophys. Res. Lett.* **40**, 3111–3117 (2013).

Methods

Ice velocity observations

We exploit 10,434 Sentinel-1a and -1b synthetic aperture radar (SAR) image pairs acquired over the west AP from December 2014 to May 2021. To improve data processing efficiency, every interferometric wide swath mode single look complex image was cropped to the dimensions of the drainage basin for each glacier (Extended Data Fig. 1a)[70,73], before the displacement of surface features was tracked using the intensity cross-correlation technique[20,74]. Velocity tracking on the AP is particularly challenging because of the steeply sloping terrain, the small size of the glaciers (56.6% in our study are less than 3 km wide near the terminus), and the extreme weather conditions including high snowfall and surface melt, which alter the radar backscatter amplitude over the 6- or 12-day temporal baseline for each pair. This increases the difficulty of recognizing and tracking the displacement of features in sequential images. Ice speed measurements were posted on a 100 m grid and a spatially variable velocity error (Extended Data Fig. 2a) was calculated by multiplying the signal-to-noise ratio of the cross-correlation with the ice speed (Fig. 1a)[20,75].

Time series of ice speed

Ice speed time series were extracted from 105 glaciers and their major tributaries from the tip of Trinity Peninsula to Sirocco Glacier in the south, in order to evaluate sub-annual change in velocity. Sample points were selected on glaciers up to −70° S with a drainage area greater than 50,000 km^2 (ref. [70]), excluding slow-moving ice piedmonts or regions where radar shadow or layover prevents good measurement coverage (Extended Data Fig. 1a). Points were located 1 km inland of the May 2021 calving front position or the most inland calving front on record to ensure that sample points were located on grounded ice while maximizing measurement coverage. The grounding line position of glaciers on the west AP is poorly known due to the difficulty in collecting measurements, lack of interferometric SAR coherence and the steep topography, with many small glaciers that must be individually characterized. The MEaSUREs[76] and ASAID[77] grounding line datasets suggest that of our eight highlight glaciers, Fleming (MEaSUREs and ASAID), Trooz and Cadman (ASAID only) Glaciers have small floating ice tongues. For all 105 glaciers, points are all inland of the MEaSUREs grounding line.

We used a single sample point rather than a larger region because of the narrow width of many glaciers on the west AP, with an average width at the terminus of 3.0 km across all 105 glaciers in the study region. We sensitivity tested these results by also extracting data from a 500 × 500 m and 1,100 × 1,100 m grid, which showed a mean difference of −7.90 m yr^{-1} and −56.83 m yr^{-1}, respectively, averaged across all glaciers on the west AP. The larger difference for the 1,100 × 1,100 m grid is attributed to the impact of including data from off-glacier and slower-flowing regions outside the main trunk on narrow glaciers. To assess whether the observed seasonal signal is sensitive to the choice of sampling strategy, we compared the ice speed anomaly in the three sampling regimes. We find the mean difference in ice speed anomaly from the sample point data was 0.63 m yr^{-1} and −0.34 m yr^{-1} for the for 500 × 500 m and 1,100 × 1,100 m grids, respectively, showing that the magnitude and timing of ice velocity fluctuations is consistent.

A Bayesian recursive smoother[78–80] was applied to each ice velocity time series to produce a daily speed estimate and corresponding uncertainty, while accounting for the measurement error, and statistics for each glacier were calculated from this dataset (Extended Data Fig. 3). The result shows how this post-processing step substantially reduces the uncertainty on ice speed throughout the time series, enabling speed change signals to be more clearly resolved above the measurement noise.

Impact of radar penetration on ice velocity measurements

Radar instruments penetrate the glacier's snowpack, unlike optical or laser instruments, which use visible light and therefore reflect off the snow surface. The depth that the radar penetrates (otherwise known as the scattering horizon) can vary in both space and time, but is primarily affected by the density of the snowpack and the presence of liquid meltwater. When there is surface melt, the scattering horizon will raise closer to the snow surface, which given the side-looking geometry of the radar instrument can induce an apparent small change in horizontal motion in the radar line of sight. As this is not related to the displacement of ice, this horizontal motion is a processing artefact and should not be misinterpreted as a real change in ice speed. This artefact only affects the range direction (line-of-sight) component of the two-dimensional velocity field, not the azimuth (along-track component), and it can only occur when there is a difference in the scattering horizon between two images—that is, once the scattering horizon has raised (or lowered), there will be no artefact in the velocity measurement. Previous studies[49] have discussed the possible impact of surface-melt-induced radar scattering horizon effects on ice velocity measurements from SAR data, specifically in relation to short-lived (six-day) acceleration events on the AP[48].

There are a number of reasons why it is unlikely that the speed change reported here is impacted by radar scattering horizon processing artefacts. First, our results (Extended Data Fig. 3) show that increased speeds are observed over a sustained period, approximately three months in the summer, which given the weekly repeat observations equates to approximately 15 independent measurements clearly documenting the increase and decrease in speed. Such increases and decreases in speed over several successive measurements could not be caused by a radar scattering horizon effect. Second, previous studies[49] have shown that the look direction of the image acquisition will influence the sign (and magnitude) of the speed change attributed to a scattering-horizon-induced artefact. For example, due to the east–west look direction of Sentinel-1 acquisitions in the northern AP region, summer melting would induce a speed decrease by raising the radar scattering horizon on glaciers on the west AP coastline such as Cayley Glacier[49]; however, we observe summertime acceleration in the same region. We also make use of ice velocity tracking data from multiple Sentinel-1 frames and viewing angles across the study area, and in some cases for the same glacier if it is covered by multiple frames, thereby reducing the impact of geometry-influenced processing artefacts should they be present. Finally, as described above, we use a Bayesian recursive smoother to produce the most likely estimate for ice speed in our time series given the measurement error[20,75], therefore our results are much less susceptible to individual anomalous velocity tracking results.

Statistical assessment of ice speed periodicity

We used a statistical assessment to determine the magnitude and periodicity of intra-annual speed variations in the Bayesian-smoothed time series from all 105 west AP glaciers (Fig. 2). Each Bayesian-smoothed ice speed time series was detrended using a third-order polynomial to remove multi-year signals, then divided into yearly segments from 1 July to 30 June. Within each year, we take the total variability (minimum to maximum) and IQR of the time series in absolute terms and normalized as a percentage of the mean speed. We assessed the annual self-similarity of each speed time series by calculating the autocorrelation at lags of one to five years, and we calculated the mean of these yearly autocorrelation values to give a single statistic per glacier for the whole six-year study period. High autocorrelation values indicate that a glacier has strong annual periodicity in its ice speed time series, whereas the IQR indicates that the corresponding glacier has a large-amplitude speed variability. This method was chosen over other frequency-based analyses as it requires no prior assumptions about the shape of the signal's waveform.

The formula used for autocorrelation (r_k) of a function y for lag k is:

$$r_k = \frac{c_k}{c_0} \times \frac{T-k}{T}$$

$$c_k = \frac{1}{T}\sum_{t=1}^{T-k}(y_t - \bar{y})(y_{t+k} - \bar{y})$$

where T is the number of samples in the time series, c_0 is the sample variance and t is an index we sum over, as defined in previous work[81].

Environmental forcing data

To investigate the availability of surface water on the west AP during the study period, we extracted daily estimates of snowmelt and rainfall from the RACMO2.3p2 regional climate model (Fig. 2)[43,52]. While the spatial resolution of the regional climate model is relatively high (5.5 km), the small size of the glaciers in the AP study region may limit the accuracy with which the climatology of an individual glacier can be resolved. We combine both rainfall and snowmelt data, as these variables represent liquid water availability at different times of the summer and have been shown to impact the speed of ice flow in Greenland[82]. The surface hydrology data provide a reliable estimate of the onset, magnitude and duration of the annually variable summer melt season, and enable differences in the spatial pattern to be resolved along the 1,000-km-long west AP coast.

We used the GLORYS12V1 European Commission Copernicus Marine Service global ocean eddy-resolving (1/12° horizontal resolution, 50 vertical levels) reanalysis model[56] to evaluate ocean temperature variability in the Bellingshausen Sea between 2014 and 2021 (Figs. 1b and 2). While ice thickness at the grounding line is highly uncertain on the AP due to the complex terrain and a paucity of bed elevation measurements, we aim to assess the temperature variability of ocean water in contact with the ice. We extracted monthly potential temperature data in the region between our ice speed sample points and 30 km offshore, or as far as islands and channels would allow. The depth-averaged temperature anomaly in the top 110 m of the water column was then calculated relative to the 2015 to 2020 mean, and we detrended the upper-ocean temperature anomaly time series using a third-order polynomial fit to remove any long-term trend in ocean heat change. This depth is chosen to capture temperature fluctuations on a seasonal scale, to give fair comparison where glacier grounding depths are largely unknown. Previous studies in other regions have shown that glacier frontal ablation rates are strongly correlated with ocean temperature at a depth of 20–60 m[62]. Finally, we measured the IQR for each complete year and averaged this to give a single seasonal ocean temperature variability value per grid cell, which provides information on the interannual seasonal ocean temperature variability (Fig. 1b).

Calving front location

We measured the change in calving front position on eight highlight glaciers with substantial speed variability, by manually digitizing the terminus location in Sentinel-1 images using the GEEDiT digitization tool (Fig. 2)[59]. Time series were produced at the highest spatiotemporal resolution possible by digitizing the whole archive of ~weekly Sentinel-1 images for each of these glaciers, at the resolution of the Sentinel-1 ground range detected product (±10 m). Change in terminus position was calculated using a curvilinear box with a 1 km width using the MaQiT tool.

Ice discharge budget and mass balance estimates

We calculate ice discharge from selected glaciers by integrating ice velocity across a flux gate defined at 1 km inland from the terminus, to ensure ice speed is extracted from the grounded ice. Flow direction is taken from the MEaSUREs ice speed mosaic dataset[83], and ice thickness was calculated from the difference between the bed elevation[39] and the ice surface elevation[71]. We assume a constant surface elevation during our study period; however, we apply a time-varying firn air content correction from the RACMO2.3p2 27 km firn densification model[52]. Ice discharge was calculated using the fully integrated time series from 1 January 2016 to 31 December 2020, followed by an ice discharge estimate using summertime-only ice speeds, which was calculated by linearly interpolating ice speed between annual summer maximums (Extended Data Table 1). Surface mass balance was calculated from RACMO2.3p2 AP 5.5 km[43,84], using drainage basins defined by ref. [70]. For Hotine Glacier (Fig. 2d), we calculate surface mass balance for the shared Hotine/Leay Glacier drainage basin.

Data availability

Source data used in this study are available as follows: Copernicus Sentinel-1A/B, available directly from the European Space Agency (https://scihub.copernicus.eu/); Copernicus Marine Service GLORYS12V1 global ocean physics reanalysis data (https://doi.org/10.48670/moi-00021); REMA Antarctic DEM V1 (https://doi.org/10.7910/DVN/SAIK8B); International Bathymetric Chart of the Southern Ocean V1.0 (https://ibcso.org/previous_releases/, https://doi.org/10.1002/grl.50413); and glacier basin inventory (https://doi.org/10.1017/S0954102014000200).

Data produced during this study are available at https://doi.org/10.5281/zenodo.7521416. This includes ice speed time series for all glaciers, calving front positions for eight highlight glaciers, glacier drainage basin scale ice velocity for eight highlight glaciers and RACMO regional climate model data.

References

73. Zwally, H. J., Giovinetto, M. B., Beckley, M. A. & Saba, J. L. *Antarctic and Greenland Drainage Systems* (GSFC Cryospheric Sciences Laboratory, 2012); https://earth.gsfc.nasa.gov/cryo/data/polar-altimetry/antarctic-and-greenland-drainage-systems
74. Strozzi, T., Luckman, A., Murray, T. & Wegmuller, U. Glacier motion estimation using SAR offset-tracking procedures. *IEEE Trans. Geosci. Remote Sens.* **40**, 2384–2391 (2002).
75. Lemos, A., Shepherd, A., McMillan, M. & Hogg, A. E. Seasonal variations in the flow of land-terminating glaciers in central-west Greenland using Sentinel-1 imagery. *Remote Sens.* **10**, 1878 (2018).
76. Rignot, E., Mouginot, J. & Scheuchl, B. *MEaSUREs Antarctic Grounding Line from Differential Satellite Radar Interferometry, Version 2*(NASA National Snow and Ice Data Center Distributed Active Archive Center, 2016); https://doi.org/10.5067/IKBWW4RYHF1Q
77. Bindschadler, R. et al. Getting around Antarctica: new high-resolution mappings of the grounded and freely-floating boundaries of the Antarctic Ice Sheet created for the International Polar Year. *Cryosphere* **5**, 569–588 (2011).
78. Kalman, R. E. A new approach to linear filtering and prediction problems. *J. Basic Eng.* **82**, 35–45 (1960).
79. Kalman, R. E. & Bucy, R. S. New results in linear filtering and prediction theory. *J. Basic Eng.* **83**, 95–108 (1961).
80. Rauch, H. E., Tung, F. & Striebel, C. T. Maximum likelihood estimates of linear dynamic systems. *AIAA J.* **3**, 1445–1450 (1965).
81. Box, G. E. P., Jenkins, G. M. & Reinsel, G. C. *Time Series Analysis: Forecasting and Control* (Prentice Hall, 1994).
82. Doyle, S. H. et al. Amplified melt and flow of the Greenland Ice Sheet driven by late-summer cyclonic rainfall. *Nat. Geosci.* **8**, 647–653 (2015).
83. Rignot, E., Mouginot, J. & Scheuchl, B. *MEaSUREs InSAR-Based Antarctica Ice Velocity Map, Version 2* (NASA National Snow and Ice Data Center Distributed Active Archive Center, 2017); https://doi.org/10.5067/D7GK8F5J8M8R
84. Rignot, E. et al. Four decades of Antarctic Ice Sheet mass balance from 1979–2017. *Proc. Natl Acad. Sci. USA* **116**, 1095–1103 (2019).

Acknowledgements

This work was led by the School of Earth and Environment at the University of Leeds. Data processing was undertaken on ARC3, part of

the high-performance computing facilities at the University of Leeds, UK. The authors gratefully acknowledge the European Space Agency and the European Commission for the acquisition and availability of Sentinel-1 data and the use of datasets produced through the Copernicus Marine Service. We also acknowledge the Polar Geospatial Center at the University of Minnesota for the availability of the REMA DEM and J. Lea of the University of Liverpool for the public availability of the GEEDiT and MaQiT digitization tools. B.J.W. is supported by the Panorama Natural Environment Research Council (NERC) Doctoral Training Partnership (DTP), under grant NE/S007458/1. A.E.H. and B.J.D. are supported by the NERC DeCAdeS project (NE/T012757/1) and ESA Polar+ Ice Shelves project (ESA-IPL-POE-EF-cb-LE-2019-834). M.R.v.d.B. was supported by the Netherlands Earth System Science Centre (NESSC). J.M.v.W. was supported by the Netherlands Organisation for Scientific Research (NWO) VENI grant VI.Veni.192.083.

Author contributions

B.J.W. and A.E.H. designed this study. B.J.W. processed the ice velocity data from the Sentinel-1 imagery and performed the analysis on all datasets. J.M.v.W. and M.R.v.d.B. produced the regional climate model data. B.J.D. extracted the ocean temperature data. B.J.W. and A.E.H. wrote the manuscript. All authors contributed to scientific discussion, interpretation of the results and contributed to the manuscript.

Competing interests

The authors declare no competing interests.

Additional information

Extended data is available for this paper at https://doi.org/10.1038/s41561-023-01131-4.

Correspondence and requests for materials should be addressed to Benjamin J. Wallis.

Peer review information *Nature Geoscience* thanks Shin Sugiyama and the other, anonymous, reviewer(s) for their contribution to the peer review of this work. Primary Handling Editor: James Super, in collaboration with the *Nature Geoscience* team.

https://doi.org/10.1038/s41561-023-01131-4

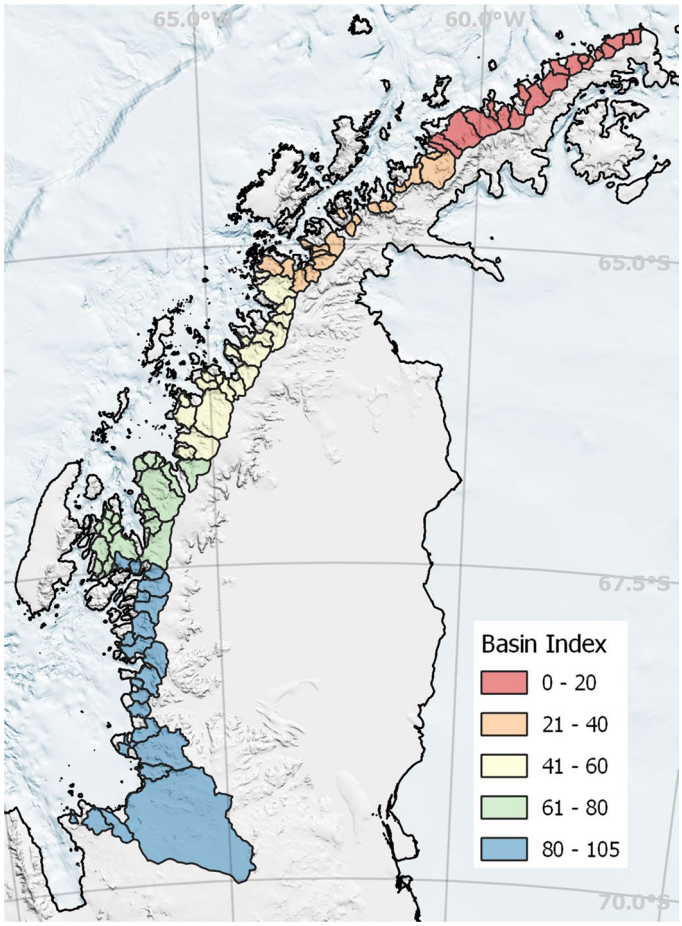

Extended Data Fig. 1 | Map of west Antarctic Peninsula glacier drainage basins. Map of west Antarctic Peninsula (AP) glacier drainage basin ID's[70], numbered 1 to 105 running from north to south. The REMA Antarctica 200 m DEM hill shade, coastline (black line) and bathymetry from IBCSO v1 are also shown[71,72].

https://doi.org/10.1038/s41561-023-01131-4

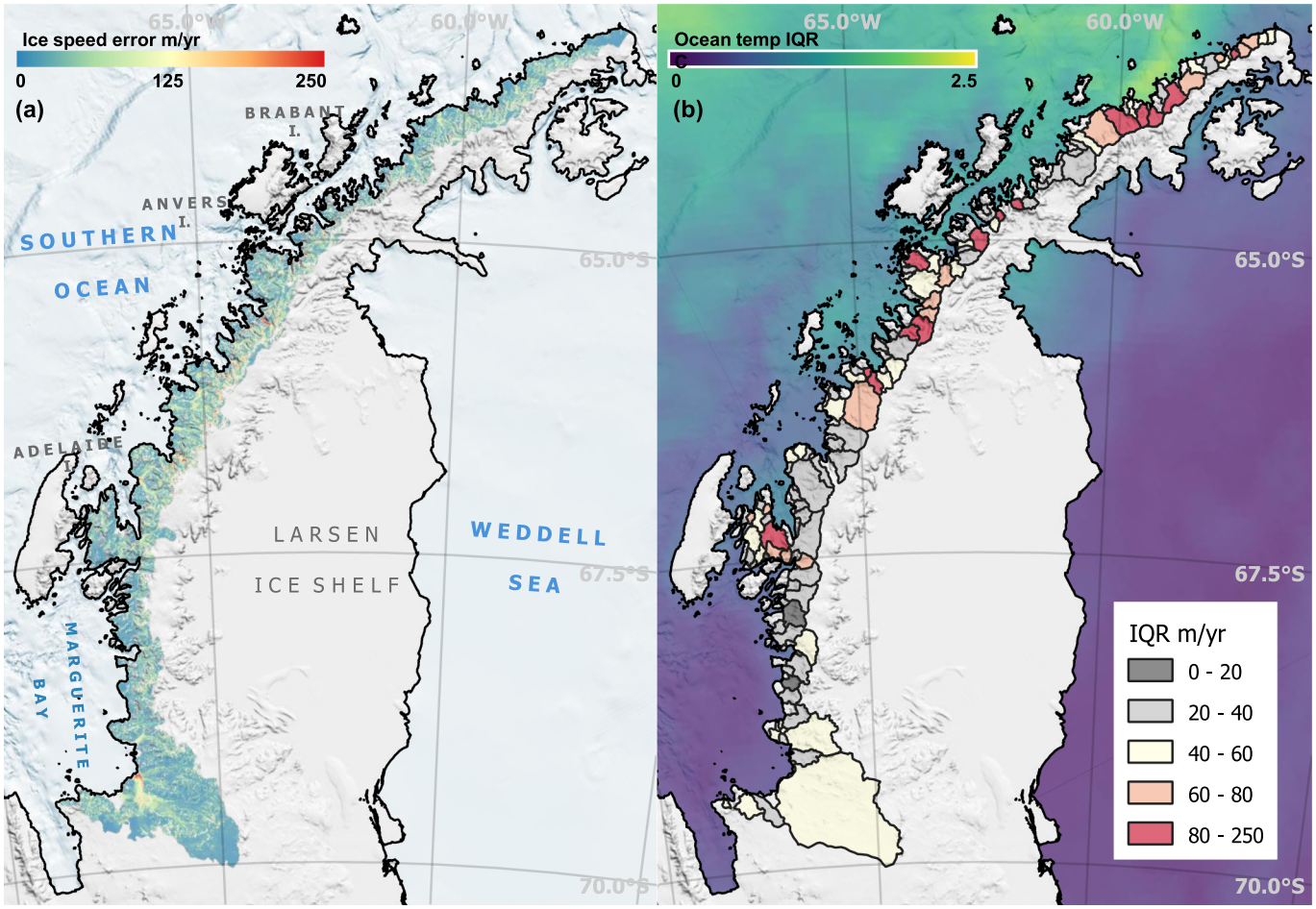

Extended Data Fig. 2 | West Antarctic Peninsula ice speed error map and speed interquartile range. a) Ice velocity error map (m/yr) on the west AP and b) Glacier drainage basins[70] shaded by the mean annual ice velocity interquartile range (IQR), which indicates high amplitude (red) and low amplitude (light grey) variability. Inter-annual upper ocean temperature variation is also shown, measured as the annual interquartile range of the depth averaged temperature anomaly in the top 110 m of the water column[56]. The REMA Antarctica 200 m DEM hill shade[71], coastline (black line) and bathymetry from IBSCO v1[72] is shown on both maps.

https://doi.org/10.1038/s41561-023-01131-4

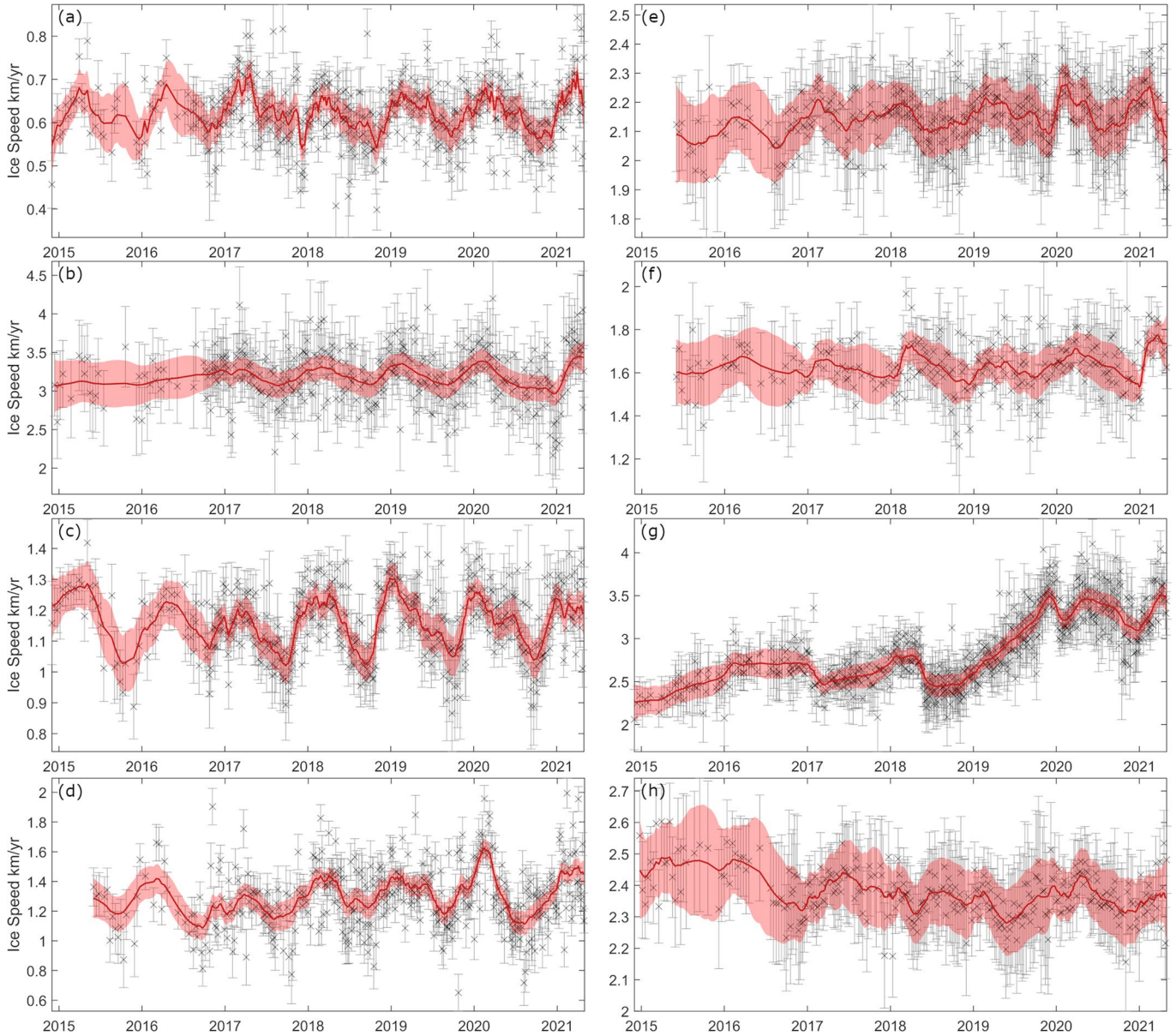

Extended Data Fig. 3 | Highlight glaciers time series of ice speed. Time-series of ice speed for 8 highlight glaciers (Fig. 2a-h). Velocity tracking measurements from individual image pair are shown as grey cross and whiskers, where the central cross is the magnitude of the velocity measurement and the central date of the image pair, and the error bar is the ice velocity tracking error defined by Lemos et al. 2018 (see Methods). Red line and shading show the Kalman smoothed speed estimate (red line) with its 95% confidence interval (light red shaded area). Time-series are shown for: a) unnamed North Bone Bay (Fig. 2a, 9), b) Gavin Ice Piedmont (Fig. 2b, 11), c) Leonardo (Fig. 2c, 27), d) Hotine (Fig. 2d, 39), e) Trooz (Fig. 2e, 42), f) Keith (Fig. 2f, 58), g) Cadman (Fig. 2g, 45) and h) Fleming (Fig. 2h, 100) Glaciers. Glaciers 'a' to 'f' were selected because of their high magnitude seasonal ice speed variability, (autocorrelation values of 0.648, 0.314, 0.586, 0.703, 0.575, 0.575 respectively) while Fleming and Cadman Glaciers were selected because of their recent longer-term ice dynamic change. We showcase a range of mean ice speeds and locations across the west AP.

https://doi.org/10.1038/s41561-023-01131-4

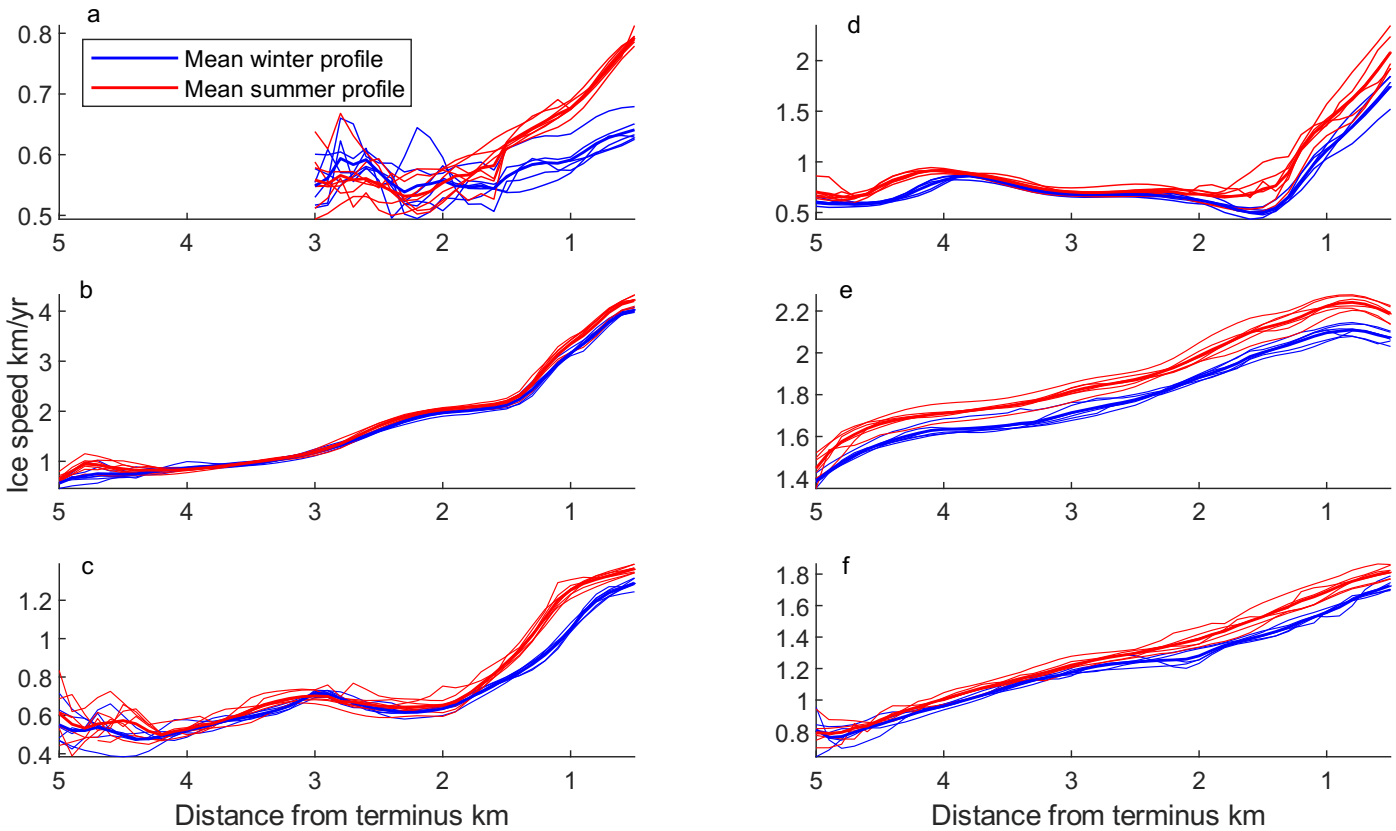

Extended Data Fig. 4 | Highlight glacier summer and winter flow profiles. Flow-line profile of mean summer (red) and winter (blue) ice speeds, where the 6-year long record of annual speeds (thin line) and the 6-year average (thick line) are both shown. Profiles were extracted when the annual maximum and minimum speeds are measured for each year. Data is shown for 8 highlight glaciers: Flow-line profiles are shown for: a) unnamed North Bone Bay (Fig. 2a, 9), b) Gavin Ice Piedmont (Fig. 2b, 11), c) Leonardo (Fig. 2c, 27), d) Hotine (Fig. 2d, 39), e) Trooz (Fig. 2e, 42), f) Keith (Fig. 2f, 58). Profiles are shown from 0.5 km to 5 km from the terminus.

https://doi.org/10.1038/s41561-023-01131-4

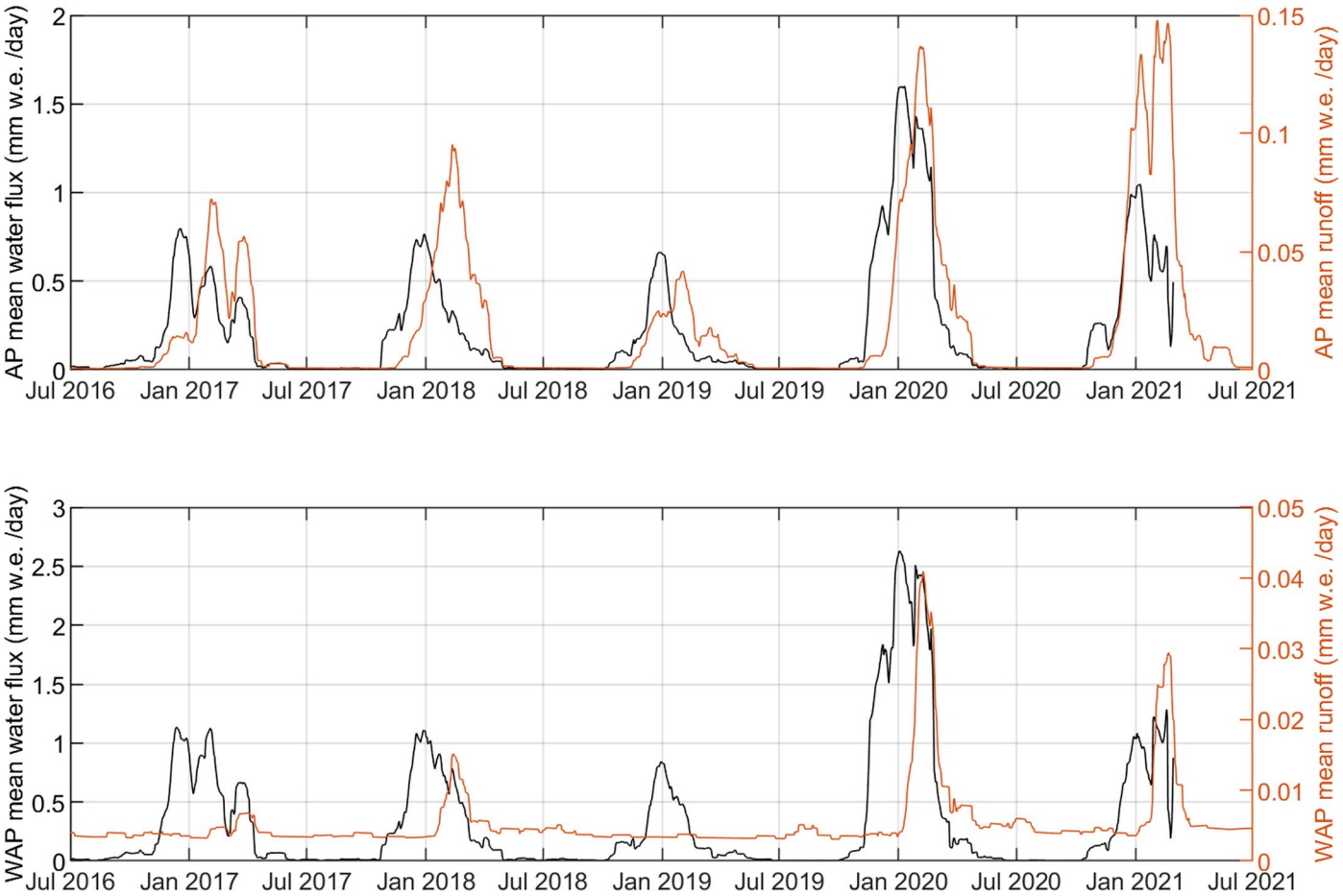

Extended Data Fig. 5 | Antarctic Peninsula scale modelled surface water flux and runoff. Modelled surface water flux (snowmelt plus rain) (black) and water runoff (orange) for RACMO2.3p2 over the whole model Antarctic Peninsula domain (upper) and the west AP drainage basin[73] (lower).

https://doi.org/10.1038/s41561-023-01131-4

Extended Data Table. 1 | Ice discharge and mass balance for 6 highlight glaciers

Glacier	Ice Discharge Gt/yr	Ice Discharge with summer speeds Gt/yr	Ice Discharge change	SMB Gt/yr	MB Gt/yr	MB with summer speeds Gt/yr	MB change
a) N. Bone Bay	0.598 ± 0.237	0.625 ± 0.248	-4.58 %	0.520 ± 0.076	-0.078 ± 0.249	-0.105 ± 0.259	35.1 %
b) Gavin Ice Piedmont	1.186 ± 0.473	1.232 ± 0.491	-3.85 %	1.380 ± 0.203	0.194 ± 0.515	0.148 ± 0.531	23.5 %
c) Leonardo	0.352 ± 0.036	0.377 ± 0.039	-6.90 %	0.475 ± 0.070	0.123 ± 0.079	0.099 ± 0.080	19.7 %
d.1) Hotine	0.434 ± 0.176	0.476 ± 0.192	-9.48 %				
d.2) Leay	0.623 ± 0.271	0.698 ± 0.304	-12.12 %				
d) Hotine + Leay	1.057 ± 0.323	1.174 ± 0.357	-11.04 %	1.236 ± 0.182	0.179 ± 0.371	0.062 ± 0.403	65.2 %
e) Trooz	2.578 ± 0.523	2.691 ± 0.552	-4.37 %	1.962 ± 0.288	-0.617 ± 0.603	-0.730 ± 0.623	18.3 %
f) Keith	1.464 ± 0.394	1.511 ± 0.407	- 3.17 %	1.227 ± 0.180	-0.237 ± 0.433	-0.283 ± 0.445	19.6%

Ice discharge and mass balance for 6 highlight glaciers (Fig. 2a-f), when using the annually variable ice speed, and assuming the summer maximum speed is sustained all year. Hotine glacier shares a drainage basin with neighbouring Leay glacier in our dataset, so mass balance is calculated for the whole basin using ice discharge across both outlets. Surface mass balance (SMB) taken from RACMO2.3p2 AP 5.5 km[45]. The error term in ice discharge is dominated by uncertainties in the bed elevation dataset (Huss & Farinotti 2014)[41] which are up to 39%. Error terms in SMB are taken from Rignot 2019[83].